Microstructure Formation and Kinetics in the Random Sequential Adsorption of Polydisperse Tethered Nanoparticles Modeled as Hard Disks

Jeffrey J. Gray,[†,||] D. Harley Klein,[†] Brian A. Korgel,*[,†,‡,§] and Roger T. Bonnecaze*[,†,‡,§]

Department of Chemical Engineering, Texas Materials Institute, and Center for Nano- and Molecular Science and Technology, The University of Texas at Austin, Austin, Texas 78712-1062

Received July 20, 2000. In Final Form: January 26, 2001

Nanotechnological applications have been proposed which require components to self-assemble into mesoscale structures. For example, nanoscale sensors, quantum memory devices, or photonic materials might comprise regular arrays of particles assembled on a substrate. Previously, we studied the random sequential adsorption kinetics and the structural phase behavior of a two-dimensional model of particles (hard disks) tethered to a substrate. The tethers restrict particle surface mobility which affects the nonequilibrium phases of the developing monolayer adsorbed to the surface. Here, we explore the effect of Gaussian polydispersity on the tethered random sequential adsorption process. Liquid, hexatic, and crystal phases are observed in the simulations. For size-monodisperse systems, short tethers (one particle radius or less) allow only liquid structures, intermediate tethers (one to four particle radii) allow a hexatic structure at high coverages, and long-tethered systems develop through liquid and hexatic phases before becoming crystalline at high coverages. Polydispersity disrupts the order. Systems over approximately 8% polydispersity remain liquid, and systems between about 7 and 8% polydispersity form a hexatic phase even with very long tethers. For sufficiently long tethers, crystal formation requires 5−7% polydispersity or less. Histograms of particle size distributions on the surface reveal that short-tether systems yield bimodal distributions because of the persistence of small gaps in the layer. In contrast, systems with adequate surface mobility organize locally, which prevents small gaps and retains unimodal size distributions. Kinetics for polydisperse, tethered, random sequential adsorption processes follow a power law with constants that change rapidly for tether lengths less than one particle radius and polydispersities up to 10%. Jamming limit coverages generally increase with polydispersity but decrease as surface order is destroyed.

I. Introduction

Many developments in nanotechnology rely on the ability to regulate the self-assembly of nanoscopic components into mesoscale structures of technological interest. Regular arrays of spheres, for example, might provide the basis for new sensor or quantum memory devices. These architectures typically require intimate and robust attachment of particles to a substrate to provide reliable physical and/or electrical substrate-to-particle connections.[1] Experimentally, chemical tethering has been realized with functionalized hydrocarbon chains to link nanocrystals to solid substrates.[2,3] In these systems, a substrate is exposed to a solution containing nanocrystals which adsorb sequentially to the surface (Figure 1). Tethering frustrates order unless the tether can provide particles with diffusional freedom along the surface. We recently used a simple two-dimensional model to show that superlattice organization depends on the ratio of tether length to particle size; the tether length controls the particle entropy and tunes the system from nonequilibrium or kinetic behavior (limited diffusional freedom) to equilibrium behavior (infinite diffusional freedom).[4] Zero tether length is a completely kinetic process called random sequential adsorption (RSA).[5] An "infinite" tether length allows free diffusion on the surface, which enables equilibrated structure formation, except for the constant perturbations of newly added particles. Our work on systems of monodisperse hard disks showed that the tether

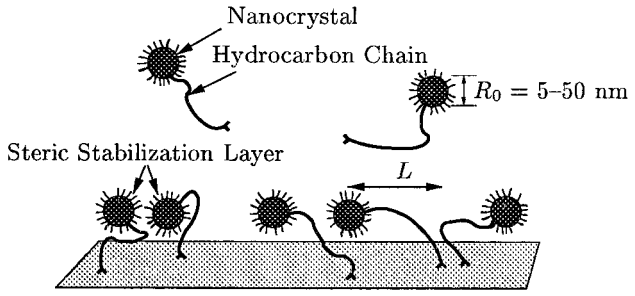

Figure 1. Adsorption of tethered nanoparticles. Steric stabilization prevents particle aggregation and irreversible "sticking" to the substrate. Van der Waals interactions keep the particles in contact with the substrate, forming a pseudo-two-dimensional system. Each particle has a tether with a functional group that can attach to the substrate and form an anchor. The tether restricts particle mobility to within a circle of radius L.

* To whom correspondence should be addressed. E-mail: korgel@che.utexas.edu and rtb@che.utexas.edu.
† Department of Chemical Engineering.
‡ Texas Materials Institute.
§ Center for Nano- and Molecular Science and Technology.
|| Present address: Department of Biochemistry, University of Washington, Seattle, WA 98195. E-mail: jjgray@u.washington.edu.

(1) Collier, C. P.; Vossmeyer, T.; Heath, J. R. *Annu. Rev. Phys. Chem.* **1998**, *49*, 371−404.
(2) Colvin, V. L.; Goldstein, A. N.; Alivisatos, A. P. *J. Am. Chem. Soc.* **1992**, *114*, 5221−5230.
(3) Andres, R. P.; Bein, T.; Dorogi, M.; Feng, S.; Henderson, J. I.; Kubiak, C. P.; Mahoney, W.; Osifchin, R. G.; Reifenberger, R. *Science* **1996**, *272*, 1323−1325.
(4) Gray, J. J.; Klein, D. H.; Bonnecaze, R. T.; Korgel, B. A. *Phys. Rev. Lett.* **2000**, *85* (21), 4430−4433.
(5) Feder, J. *J. Theor. Biol.* **1980**, *87*, 237.

10.1021/la001029j CCC: $20.00
Published on Web 03/16/2001

length controls the final morphology of an adsorbed particle layer between a disordered liquid phase, a hexatic phase, or an ordered crystalline phase. The kinetics of the system follow asymptotic, long-time power-law behavior with rate constants dependent on tether length. One issue inherent in the experimental realization of nanoparticle systems is that it can be difficult to create narrow particle size distributions. Size polydispersity disrupts order formation, and approximately 10% polydispersity (measured as the standard deviation of particle size divided by the mean) is the "rule of thumb" upper limit for order formation.[6] In this paper, we study the effect of polydispersity on tethered RSA of nanoparticles.

Polydispersity effects have been studied in both equilibrium and RSA systems. In equilibrium systems, studies have focused on equations of state and the structure of the two-dimensional system of disks. Alder and Wainwright's 1962 molecular dynamics study pioneered the simulation of the phase transition in hard disks, finding a hysteresis loop in the pressure−area curve for fractional surface coverages ranging from 68 to 72%, corresponding to the order−disorder transition.[7] Recently, increased computer power and more refined knowledge of two-dimensional phase transitions have fueled debate about the exact nature of the phase transition, specifically, whether it includes a hexatic phase between the fluid and crystal phases.[8,9] The effect of polydispersity on the phase transition has been studied for elastic disks,[10] Lennard−Jones particles,[11] and soft (r^{-12}) disks[12] for binary, uniform, triangular, and Gaussian particle distributions. These studies generally concluded that the introduction of polydispersity shifts the crystal−fluid transition to higher areal fractions[10] and at a "terminal" polydispersity δ_t, the phase transition disappears and a disordered state exists for all densities. Estimates of δ_t range from 6 to 10%. The disruption of order in an equilibrium system has been studied more extensively in three dimensions.[13−23]

Polydisperse RSA studies have concerned adsorption kinetics and jamming limit coverages. Monodisperse systems adsorb to a jamming limit of $\theta_\infty = 0.547$ according to the power law $\theta_\infty - \theta(\tau) \sim \tau^{-1/2}$, where θ is the fractional surface coverage and τ is proportional to the number of adsorption attempts.[5,24] The first studies of polydisperse RSA analytically examined binary mixtures with more than 3-fold differences in size and found that the long-time asymptotic decay of coverage to the jamming limit depends on the species: large particle adsorption decays exponentially, whereas small particle adsorption follows the $\tau^{-1/2}$ power law of classic (monodisperse) RSA.[25] The $\tau^{-1/2}$ form also holds when adsorbing large particles onto a surface pretreated with small particles.[26] For particles with uniform size distributions, derivations showed that surface coverage decays to the jamming limit as $\tau^{-1/3}$ (or $\tau^{-1/(3+n)}$ for distributions with n nonzero derivatives at the lower size limit of the distribution).[27] These decay exponents are consistent with the concept that the long-time kinetics scale as $\tau^{-1/d}$, where d reflects the degrees of freedom in the system; for example, $d = 2 + 1$ for the two-dimensional space plus the particle polydispersity. Extensive RSA simulations confirmed the validity of the derived asymptotic forms for uniform distributions and binary mixtures. For Gaussian distributions, for which a theoretical form has not been derived, simulations reveal $\tau^{-1/2}$ behavior for small polydispersities but much slower adsorption for larger distributions of particle sizes.[28,29] For power-law distributions of particles that adsorb reversibly, kinetics slow dramatically to fit a stretched exponential of the form $\exp(-\tau^{\beta})$, where β is a constant that depends on the desorption rate law.[30] In the limit of short times, the first several terms in an analytic expansion of the available surface function (useful for Langmuir type rate laws) are available for the RSA of two-component mixtures.[31] This available surface function has also been analytically expanded for (monodisperse) systems with diffusion or desorption, bridging the gap between RSA systems and equilibrium systems.[32] Finally, the jamming limit θ_∞ has been found to increase with polydispersity for uniform distributions of particles.[29]

Few classic RSA studies of polydisperse mixtures have focused on surface structure because particles stick to their original locations to produce trivially disordered monolayers. One exception is a recent study examining particles distributed with probability $\alpha R^{\alpha-1}$, where R is the particle radius and α is a positive constant.[33,34] As $\alpha \to \infty$, the organization on the surface tends toward perfect Apollonian packing, a highly organized fractal configuration with disks of progressively smaller sizes packed tightly between each of the interstices of the larger particles. These power-law distributions of particles in the bulk adsorb to a different power-law distribution on the surface.[35]

The goal of this study is to determine the effect of Gaussian polydispersity on surface morphology and kinetics of the tethered RSA process. After detailing our simulation method, we present a general overview of polydispersity effects on surface structure, including examples of the correlation functions used to characterize structures and a detail of the classification scheme used for two-dimensional nonequilibrium phases. Phase dia-

(6) Korgel, B. A.; Fitzmaurice, D. *Phys. Rev. B* **1999**, *59*, 14191−14201.
(7) Alder, B. J.; Wainwright, T. E. *Phys. Rev.* **1962**, *127*, 359−361.
(8) Jaster, A. *Phys. Rev. E* **1999**, *59*, 2594−2602.
(9) Weber, H.; Marx, D.; Binder, K. *Phys. Rev. B* **1995**, *51*, 14636−14651.
(10) Vermöhlen, W.; Ito, N. *Phys. Rev. E* **1995**, *51*, 4325−4334.
(11) Sadr-Lahijany, M. R.; Ray, P.; Stanley, H. E. *Phys. Rev. Lett.* **1997**, *79*, 3206−3209.
(12) Bocquet, L.; Hansen, J.-P.; Biben, T.; Madden, P. *J. Phys.: Condens. Matter* **1992**, *4*, 2375−2387.
(13) Dickinson, E.; Parker, R.; Lal, M. *Chem. Phys. Lett.* **1981**, *79*, 578−582.
(14) Dickinson, E.; Parker, R. *J. Phys., Lett.* **1985**, *46*, L229−L232.
(15) Barrat, J. L.; Hansen, J. P. *J. Phys.* (*Paris*) **1986**, *47*, 1547−1553.
(16) Pusey, P. N. *J. Phys.* (*Paris*) **1987**, *48*, 709−712.
(17) Moriguchi, I.; Kawasaki, K.; Kawakatsu, T. *J. Phys. II* **1993**, *3*, 1179−1184.
(18) Cottin, X.; Monson, P. A. *J. Chem. Phys.* **1993**, *99*, 8914−8921.
(19) Cottin, X.; Monson, P. A. *J. Chem. Phys.* **1995**, *102*, 3354−3360.
(20) Bolhuis, P. G.; Kofke, D. A. *Phys. Rev. E* **1996**, *54*, 634−643.
(21) Phan, S.-E.; Russel, W. B.; Zhu, J.; Chaikin, P. M. *J. Chem. Phys.* **1998**, *108*, 9789−9795.
(22) Lacks, D. J.; Wienhoff, J. R. *J. Chem. Phys.* **1999**, *111*, 398−401.
(23) Zhang, J.; Blaak, R.; Trizac, E.; Cuesta, J. A.; Frenkel, D. *J. Chem. Phys.* **1999**, *110*, 5318−5324.
(24) Swendsen, R. H. *Phys. Rev. A* **1981**, *24*, 504−508.
(25) Talbot, J.; Schaaf, P. *Phys. Rev. A* **1989**, *40*, 422−427.
(26) Adamczyk, Z.; Weroński, P. *J. Chem. Phys.* **1998**, *108*, 9851−9858.
(27) Tarjus, G.; Talbot, J. *J. Phys. A: Math. Gen.* **1991**, *24*, L913−L917.
(28) Meakin, P.; Jullien, R. *Phys. Rev. A* **1992**, *46*, 2029−2038.
(29) Adamczyk, Z.; Siwek, B.; Zembala, M.; Weroński, P. *J. Colloid Interface Sci.* **1997**, *185*, 236−244.
(30) Olson, C. B.; Talbot, J. *J. Chem. Phys.* **2000**, *112*, 3868−3874.
(31) Talbot, J.; Jin, X.; Wang, N.-H. L. *Langmuir* **1994**, *10*, 1663−1666.
(32) Tarjus, G.; Schaaf, P.; Talbot, J. *J. Chem. Phys.* **1990**, *93*, 8352−8360.
(33) Brilliantov, N. V.; Andrienko, Y. A.; Krapivsky, P. L.; Kurths, J. *Phys. Rev. Lett.* **1996**, *76*, 4058−4061.
(34) Brilliantov, N. V.; Andrienko, Y. A.; Krapivsky, P. L.; Kurths, J. *Phys. Rev. E* **1998**, *58*, 3530−3536.
(35) Semmler, M.; Ricka, J.; Borkovec, M. *Colloids Surf., A* **2000**, *165*, 79−93.

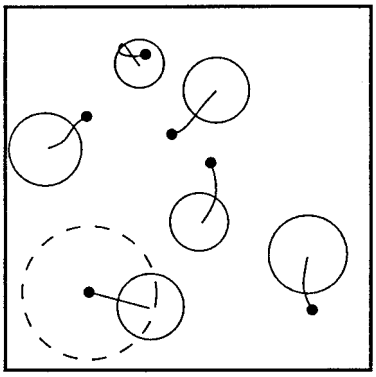

Figure 2. Polydisperse RSA with tethers. A normal distribution of hard disk particles are added sequentially in random positions as long as they do not overlap with preadsorbed particles. Particles on the surface are free to diffuse within the finite tether length from the initial adsorption location or anchor point.

grams reveal the phase behavior as a function of tether length, polydispersity, and deposition time or surface coverage. The relationship between the particle size distribution of the sample and the size distribution on the surface is also examined. Finally, kinetic analyses reveal the relationship between structure and kinetics and allow extrapolation to determine jamming coverages.

II. Method

We follow the standard RSA procedure where particles (disks) are tethered to random anchor locations in a periodically replicated square and overlapping particle placements are rejected[5] (Figure 2). The particles are modeled as hard disks because their motion is practically restricted to the plane as a result of the energy minimum determined by the balance between van der Waals attractive forces and steric repulsive forces due to the short-chain hydrocarbons between the particles and the planar surface. Our system is $100R_0 \times 100R_0$, where R_0 is the mean radius of the adsorbing particles. Incoming particle sizes are distributed normally with a fractional standard deviation of δ:

$$P(R) = \frac{1}{\sqrt{2\pi}\delta R_0} \exp[-(R - R_0)^2/2\delta^2 R_0^2] \qquad (1)$$

where $P(R)$ is the probability density of particles of radii R in the bulk of the suspension. Between adsorption attempts, particles diffuse according to a Monte Carlo scheme that adjusts step size to obtain 50% acceptance of moves.[36] Diffusion move magnitudes and directions are chosen from two independent uniform distributions, and moves that place particles outside of the finite range of the tether and those that result in particle−particle overlap are rejected. Two hundred Monte Carlo cycles (a cycle is defined as N successful moves, where N is the current number of particles on the surface) are completed after every successful adsorption and at "time" intervals of 0.0785, where the time $\tau = \gamma a/A$ is defined as the number of adsorption attempts γ scaled by the relative areas of a disk a and the simulation box A. Because most particle adsorption attempts are unsuccessful (10^{-8} success rate at long times), the rate of surface diffusion far exceeds the rate of particle addition at long times when the important phase behavior and kinetics are observed.

To accelerate computation, overlap calculations are implemented using a grid. The computational area is divided evenly into 1600 cells, and a record is kept of the particles in each cell. To determine if particle overlap occurs during a new or diffusing particle placement, it is only necessary to loop over particles in the destination cell and the neighboring eight cells. Computational times are much higher in systems with long tethers and polydisperse particles. Simulations reported here require 12−72 h each on current Unix workstations operating near 600 MHz.

III. Adsorbed Layer Morphologies

Monodisperse particles with $L/R_0 = 5$ order at high coverages (Figure 3a). Polydispersity frustrates order: at a polydispersity of $\delta = 0.05$ (Figure 3b), a slight "twist" occurs in the lattice directions of the adsorbed layer; at $\delta = 0.075$ (Figure 3c), the twist becomes much more dramatic, and although one can see islands of hexagonally packed disks, the larger structure lacks a dominant direction of the lattice vectors; at $\delta = 0.1$ (Figure 3d), structural organization is short-range with many obvious defects.

A quantitative description of surface structure is obtained by evaluating two correlation functions. The first of these is a translational correlation function or pair distribution function, $g(r)$, which represents particle density at a distance r from a reference particle:

$$g(r) = \frac{\langle n(r) \rangle}{n} \qquad (2)$$

where $n(r)$ is the local density at a distance r from a reference particle, brackets represent an average over the particles in the system, and n is the average particle density. The simulation computes $g(r)$ by averaging over all particles over several diffusion cycles.

Figure 4 shows $g(r)$ for $L/R_0 = 5$ as polydispersity increases. Monodisperse particles give rise to distinct peaks representative of the lattice structure on the surface. The amplitude of the peaks decays at large r because of averaging over different angles and thermal fluctuations in the system. As polydispersity increases, $g(r)$ becomes more smooth. At $\delta = 0.15$, only three broad peaks are clearly seen. Note also that the second broad peak "splits" into two peaks when $\delta \leq 0.07$. Peak-splitting can be used to approximately distinguish ordered (hexatic or crystal) from disordered phases.[37]

The second correlation function used to quantify two-dimensional surface structure is the orientational correlation function, $g_6(r)$. A complex order parameter determines the "orientation" of each particle by measuring 6-fold symmetry:

$$\psi_6^{(j)} = \frac{1}{z} \sum_k \exp(6i\phi_{jk}) \qquad (3)$$

where ϕ_{jk} is the orientation angle of the line connecting the centers of the reference disk j and each of the z neighboring disks labeled k.[38] (We define neighbors as all disks closer than $r = \sqrt{0.7/\theta}$, which corresponds roughly to the trough between the first and second peaks in $g(r)$.) The magnitude of $\psi_6^{(j)}$ reaches a maximum of unity when particle j has six neighbors, each separated by 60°; the

(36) Allen, M. P.; Tildesley, D. J. *Computer Simulation of Liquids*; Oxford University Press: Oxford, 1987.

(37) Gray, J. J. Ph.D. Thesis, The University of Texas at Austin, Austin, TX, 2000.

(38) *Bond Orientational Order in Condensed Matter Systems*; Strandburg, K. J., Ed.; Springer-Verlag: New York, 1992.

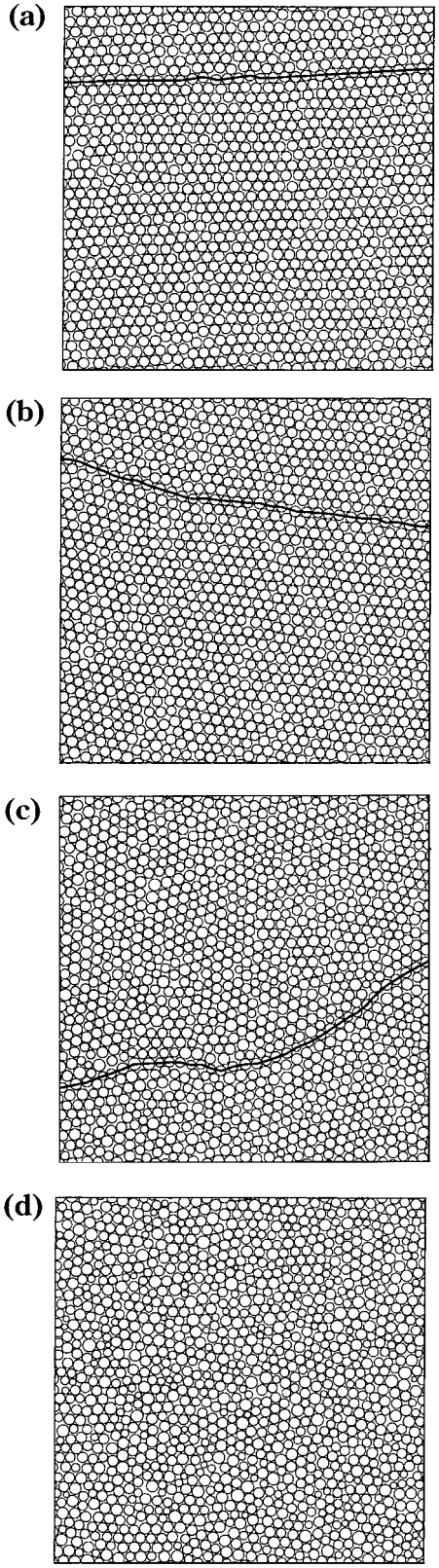

Figure 3. Surface structures created by adsorption of polydisperse tethered particles with $L/R_0 = 5$: (a) $\delta = 0$, (b) $\delta = 0.05$, (c) $\delta = 0.075$, and (d) $\delta = 0.1$. Snapshots are taken at the final simulation times of $\tau = 1.70 \times 10^5$, 4.48×10^5, 3.61×10^5, and 6.69×10^5 and surface coverages of $\theta = 0.744$, 0.752, 0.743, and 0.751, respectively. The solid lines highlight the crystalline order in (a) and the characteristic twist of the hexatic in (b) and (c).

angle of the complex vector represents the rotation of the spatial pattern of surrounding disks. The orientational

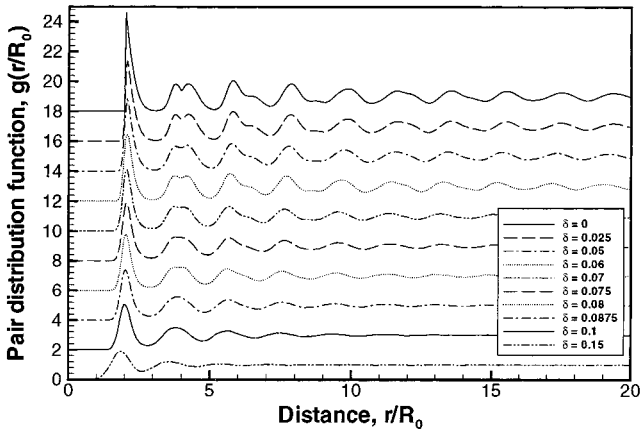

Figure 4. Pair distribution function $g(r)$ for $L/R_0 = 5$ as a function of polydispersity. Note the loss of peak-splitting in the second shell for $\delta > 0.07$. Data are evaluated at the final simulation time. For all runs represented here, $5 \times 10^5 < \tau < 5 \times 10^6$ and $0.734 < \theta < 0.745$. Curves are offset for clarity.

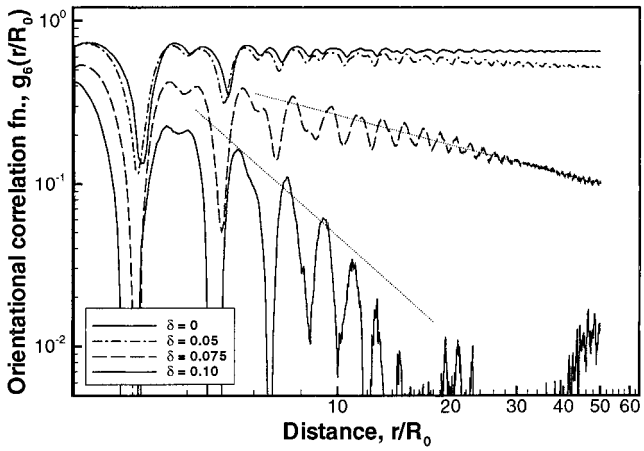

Figure 5. Orientational correlation function $g_6(r)$ for the $L/R_0 = 5$ configurations depicted in Figure 3. Dotted lines are drawn as a reference for power-law decay.

correlation function is computed analogously to $g(r)$:

$$g_6(r) = \frac{\langle \psi_6^*(0)\, \psi_6(r) \rangle}{g(r)} \tag{4}$$

where the star denotes the complex conjugate and the brackets are again an ensemble average. Like $g(r)$, $g_6(r)$ is in practice averaged over several diffusion cycles; the precise formulas used in computations are provided in the Appendix.

Figure 5 shows $g_6(r)$ for the four simulation configurations in Figure 3. For the monodisperse case, the oscillations of $g_6(r)$ decay to a constant at large r, indicating long-range orientational order. In contrast, $g_6(r)$ for the three polydisperse cases decays. At $\delta = 0.05$ and $\delta = 0.075$, $g_6(r)$ decays as a power law (linear on the logarithmic plot), with the $\delta = 0.05$ case decaying very slowly and the $\delta = 0.075$ case decaying much more rapidly. (The $\delta = 0.05$ case is near the limit of our ability to distinguish a decay of the $g_6(r)$ function; within the noise of the $g_6(r)$ oscillations, we can detect slopes down to approximately 0.02.) The correlation function for $\delta = 0.1$ decays exponentially, here seen by the faster-than-power-law decay on the logarithmic axes.

The functional decays of $g(r)$ and $g_6(r)$ reveal the phases. According to the Kosterlitz−Thouless−Halperin−Nel-

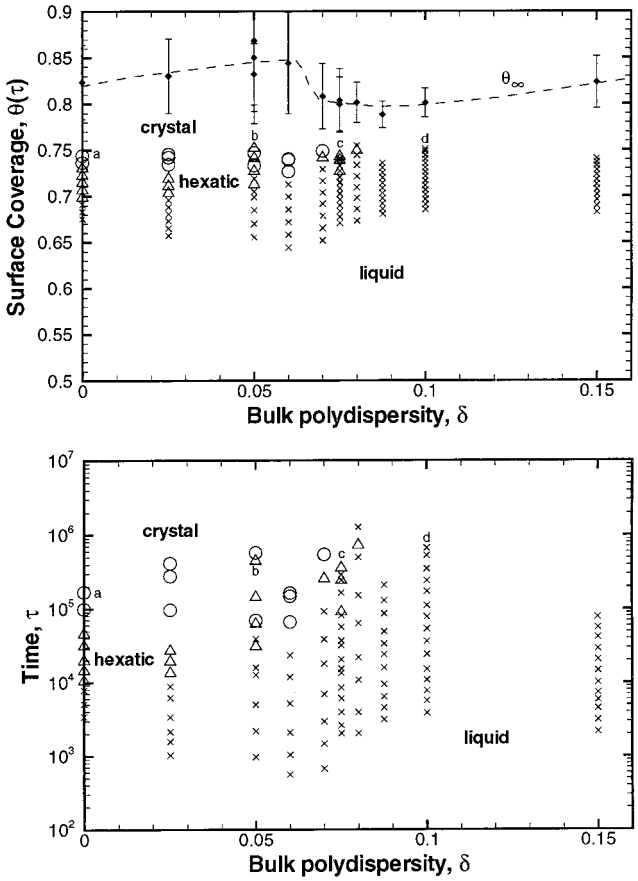

Figure 6. Phase diagrams of polydispersity versus coverage (top) and polydispersity versus time (bottom) for tether length $L/R_0 = 5$. The symbols ×, △, and ○ represent liquid, hexatic, and crystal phases, respectively. Multiple runs are superimposed at $\delta = 0.05$ and 0.075. Letters denote points corresponding to snapshots in Figure 3. Filled points are extrapolated jamming coverages (section VI).

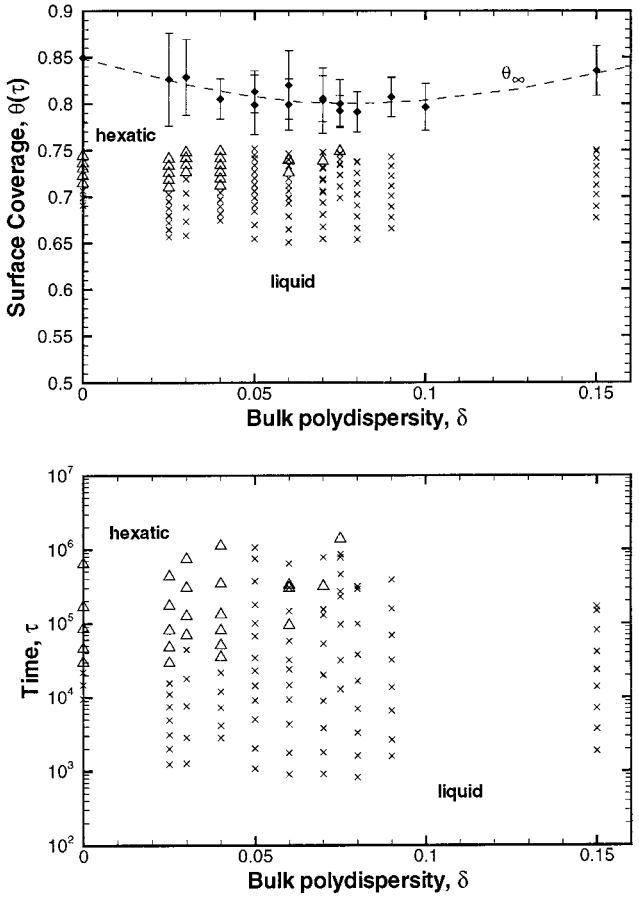

Figure 7. Phase diagrams of polydispersity versus coverage (top) and polydispersity versus time (bottom) for tether length $L/R_0 = 2$. The symbols ×, △, and ○ represent liquid, hexatic, and crystal phases, respectively. Multiple runs are superimposed at $\delta = 0.06$, 0.07, and 0.075. The upper plot includes jamming limit extrapolations (section VI).

son−Young (KTHNY) theory of phase transitions,[38−41] a two-dimensional crystal exhibits true long-range orientational order [$g_6(r) \sim$ constant] and quasi-long-range translational order [$g(r) \sim r^{-\xi}$]. A two-dimensional liquid exhibits short-range order for both the orientational and translational correlation functions [$g_6(r) \sim \exp(-\xi r)$ and $g(r) \sim \exp(-\xi r)$]. An intermediate two-dimensional hexatic phase exhibits quasi-long-range orientational order [$g_6(r) \sim r^{-\xi}$] and short-range translational order [$g(r) \sim \exp(-\xi r)$].

In this paper, we continue to use the KTHNY formalism and employ the decay rate of the $g_6(r)$ function to formally distinguish the three phases for any given surface configuration.

IV. Polydisperse Phase Behavior

Figure 6 shows the phase evolution of tethered hard disks with $L/R_0 = 5$ for various polydispersities, including the four points corresponding to Figure 3. At this long tether length, the monodisperse particles have sufficient local mobility to organize into a crystal. In a polydisperse system, crystal structures develop when $\delta \leq 0.07$, and hexatic structures develop with $\delta \leq 0.08$. Polydispersity affects the onset of structural organization, with order occurring later and at higher coverages with greater δ. Results are also history-dependent, and near the transition points multiple runs with different random number seeds do not always produce the same structures: at $\delta = 0.05$, one system crystallizes whereas another remains hexatic; at $\delta = 0.075$, one system becomes hexatic whereas another remains liquid. The $\delta = 0.08$ system becomes hexatic at $\theta = 0.749$ but loses the order at $\theta = 0.754$. For polydispersities larger than 0.08, structures are always disordered.

Figure 7 similarly shows the structural evolution for a variety of polydispersities at $L/R_0 = 2$. At this intermediate tether length, monodisperse systems cannot crystallize completely but rather become hexatic near $\theta = 0.70$ and $\tau = 3 \times 10^4$. Systems with $\delta < 0.05$ behave similarly. For $\delta \geq 0.05$, the hexatic structure is less favored. For $\delta = 0.06-0.075$, the hexatic phase does not develop until the higher coverage of approximately 0.73 and τ of 10^5-10^6. For $\delta = 0.05$, the hexatic does not appear, even at $\theta = 0.75$ and $\tau = 10^6$. For $\delta \geq 0.08$, systems are liquid for the entire duration of the simulations.

The diagrams in Figure 8 show phase behavior as the tether is varied in a modestly polydisperse system ($\delta = 0.05$). Like monodisperse systems, the polydisperse system exhibits liquid, hexatic, and crystalline phase behavior. For short tethers ($L/R_0 \leq 2$), structures are always disordered (liquid). For intermediate tethers ($3 \leq L/R_0 \leq 3.5$), the hexatic phase develops at high coverages or long times. For long tethers ($L/R_0 \geq 3.75$), the system passes through the liquid and hexatic structures before becoming crystal. Monodisperse and polydisperse systems differ in

(39) Kosterlitz, J. M.; Thouless, D. J. *J. Phys. C: Solid State Phys.* **1973**, *6*, 1181.
(40) Halperin, B. I.; Nelson, D. R. *Phys. Rev. Lett.* **1978**, *41*, 121.
(41) Young, A. P. *Phys. Rev. B* **1979**, *19*, 1855.

Table 1. Terminal Polydispersities (δ_t), above Which Only Disordered Phases Occur, from Two-Dimensional Simulation Studies

work	δ_t	particle distribution	notes
Bocquet et al., 1992 (ref 12)	10%	binary	r^{-12} interactions, $N = 108$
Vermöhlen and Ito, 1995 (ref 10)	6−7.5%	binary and uniform	Hertzian interactions
Sadr-Lahijany et al., 1997 (ref 11)	9.7%	binary	Lennard−Jones particles, hexatic trans. for low densities
Gray et al., 2001 (this work)	7% for crystal, 8% for hexatic	Gaussian	nonequilibrium, tethered system

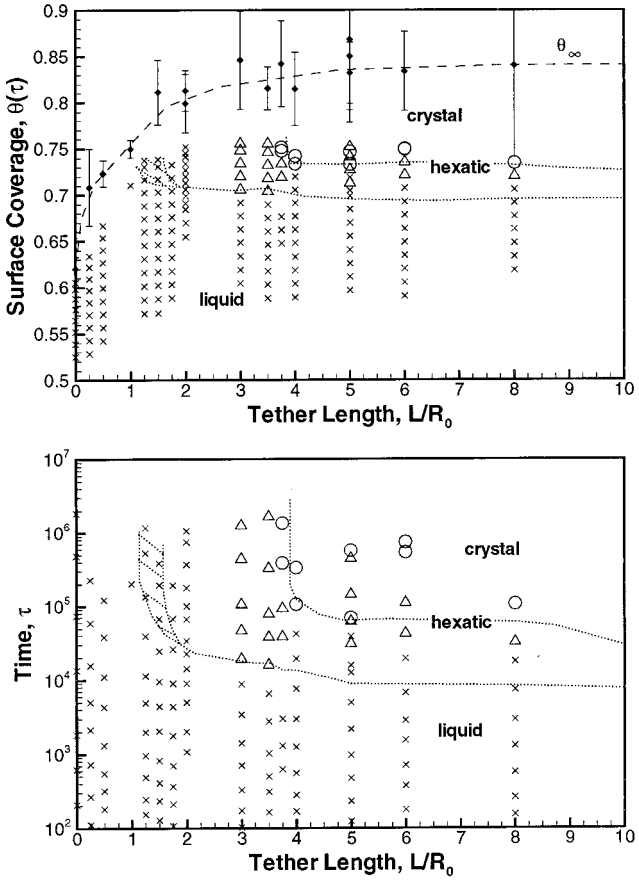

Figure 8. Phase diagrams of tether length versus coverage (top) and tether length versus time (bottom) for a polydisperse system ($\delta = 0.05$). The symbols ×, △, and ○ represent liquid, hexatic, and crystal phases, respectively. Dashed lines show the phase boundaries from the *monodisperse* system, and hatched regions indicate where both liquid and hexatic phases were observed (taken from ref 4). Points for two distinct runs are superimposed at $L/R_0 = 5$. The upper plot includes jamming limit extrapolations (section VI).

several places, as seen by comparison with the superimposed phase boundaries for a monodisperse system from ref 4. The monodisperse system exhibits a hexatic phase at the lower tether length of $L/R_0 = 1.25$. For long tethers, the polydisperse liquid becomes hexatic at longer times and higher coverages than in the monodisperse system. Also, two runs at $L/R_0 = 5$ (which use different random number seeds) show the nonequilibrium, process-dependent nature of this polydisperse system: one run becomes crystal, and the other remains hexatic at long times.

Figure 9 summarizes the final state observed in simulations as a function of both polydispersity and tether length. At high polydispersities ($\delta \geq 0.085$) or short tether lengths ($L/R_0 \leq 1$), only liquid structures are observed. For $\delta < 0.075$ and $L/R_0 > 4$, crystal structures usually form. Between these conditions, the hexatic is the final structure observed in the simulation. Note that this figure hides some of the details that are shown in the more complete earlier figures; generally, phase transitions

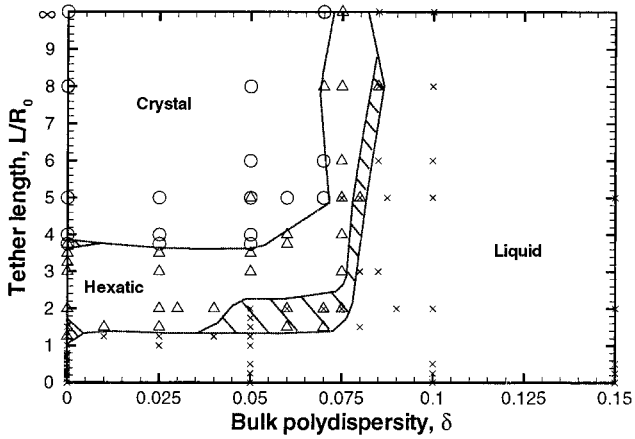

Figure 9. Polydispersity/tether length phase diagram for adsorption of polydisperse tethered particles. The symbols ×, △, and ○ represent liquid, hexatic, and crystal phases, respectively. Dashed lines represent approximate phase boundaries, and hatched regions denote uncertain areas. Note that the phase behavior reported here is for maximum practical simulation time (near $\tau = 10^6$) and that microstructure may continue to evolve in this kinetic system.

happen later and at higher coverages as polydispersity increases. In addition, in polydisperse systems some simulations behave differently depending on the random number seed chosen. The regions where final behavior is somewhat indeterminate are marked with hatched regions in Figure 9. Note that the "final" state in the simulation simply denotes a cutoff point where further simulation becomes impractical from the standpoint of time and computer resources. The surface coverage will continue to increase until reaching the jamming limit, and the possibility that different phases could be observed over a longer time scale cannot be ruled out.

Although our RSA results are *nonequilibrium* results, it is appropriate to compare our phase boundaries to corresponding equilibrium systems. Table 1 summarizes simulation studies of the ordering of polydisperse disks. Our terminal polydispersities are slightly higher than those of Vermöhlen and Ito[10] and lower than those of Bocquet et al.[12] and Sadr-Lahijany et al.[11] Our simulations differ in several ways from these studies. Because we are performing nonequilibrium simulations, our simulations may sometimes not achieve an ordered state even if that is the equilibrium morphology. Also, we simulate hard disks, and these equilibrium studies were all done for soft disks. In studies of colloidal particles that interact through the electrostatic double layer, salt concentration can tune the length scale of particle interactions, and softer particles are known to order more easily than those more like hard spheres or disks.[42] Finally, some terminal polydispersity estimates may differ because of fractionation. We report our numbers for polydispersities in the bulk, whereas the polydispersity on the surface is somewhat greater. For long tethers and polydispersities low enough to allow order,

(42) Gray, J. J.; Bonnecaze, R. T. *J. Chem. Phys.* **2001**, *114* (3), 1366−1381.

surface polydispersities are up to 1% higher than bulk polydispersities. Despite these differences between our simulations and others, the breakup of order in systems of two-dimensional disks seems to be somewhat universal in the range of 6−10% polydispersity.

The questions of how and why polydispersity disrupts order remain. Certainly, large (or small) particles can create defects. For three-dimensional systems, Pusey suggested that order will be disrupted when a significant fraction of the particles become as large as $R_{max} = r_{nn}/2$, where r_{nn} is the distance between nearest neighbors on a regular lattice.[16] If this criterion explains the breakup of order, our δ_t of 0.08 in (two-dimensional) systems ranging from $\theta = 0.7-0.75$ indicates that the fraction of particles larger than R_{max} necessary to disrupt organization is 11−14%.

V. Size Distributions in Surface Phases

The particle size distribution on the surface can change as adsorption proceeds. Figure 10 shows the evolution of the distribution for two different tether lengths at $\delta = 0.05$. For $L/R_0 = 0$, the particle distribution is nearly Gaussian with a standard deviation of 0.05 until the longest time ($\tau \approx 10^6$) when the histogram skews toward smaller particle radii and the surface polydispersity increases to near 0.07. A significant number of particles in the size regime of $0.75 \leq R \leq 0.9$ adsorb at long times. In contrast, the $L/R_0 = 5$ case remains symmetric even at the longest simulation times. The explanation can be found by visually examining the structures shown in Figure 10. As the surface becomes crowded, larger particles have a greater chance of overlap and rejection. With $L/R_0 = 0$, the immobile particles form a disordered structure with many gaps that can be filled by particles fractionally smaller than the mean size. With $L/R_0 = 5$, the surface mobility enables hexatic or crystalline restructuring, which results in few defects and fairly long-range order. The gaps in those closely packed structures cannot accommodate particles substantially smaller than the mean size. A distribution with only 5% polydispersity contains almost no particles small enough to fill these gaps.

Systems with larger polydispersity create more dramatic behavior. Figure 11 shows the evolution of particle size histograms for the larger polydispersity of $\delta = 0.15$. Short tether lengths (parts a and b of Figure 11, $L/R_0 = 0$ and 0.25, respectively) develop a bimodal distribution at long times. The primary peak shifts from the mean bulk particle size R_0 to $0.9R_0$, and a new secondary peak arises near $0.5R_0$. For longer tethers (parts c and d of Figure 11, $L/R_0 = 2$ and 5, respectively), the primary peak again shifts from R_0 to $0.9R_0$, reflecting the preferential adsorption of smaller particles that have a lower chance of overlap with preadsorbed particles. However, the distribution remains unimodal, in striking contrast to the short-tether cases. Although systems with little diffusion create disordered structures with substantial gaps that accommodate particles on the small side of the distribution (Figure 11e), systems with sufficient diffusion rearrange to pack without large gaps (Figure 11f). Even though the $L/R_0 = 2$ and 5 polydisperse systems do not order, the particles' local freedom still allows small clusters of particles to form with short-range hexagonal packing, eliminating the large gaps between particles and preventing the distribution from becoming bimodal.

Because of the preference for the adsorption of small particles, the adsorption process exacerbates the polydispersity of the system, especially for large polydisper-

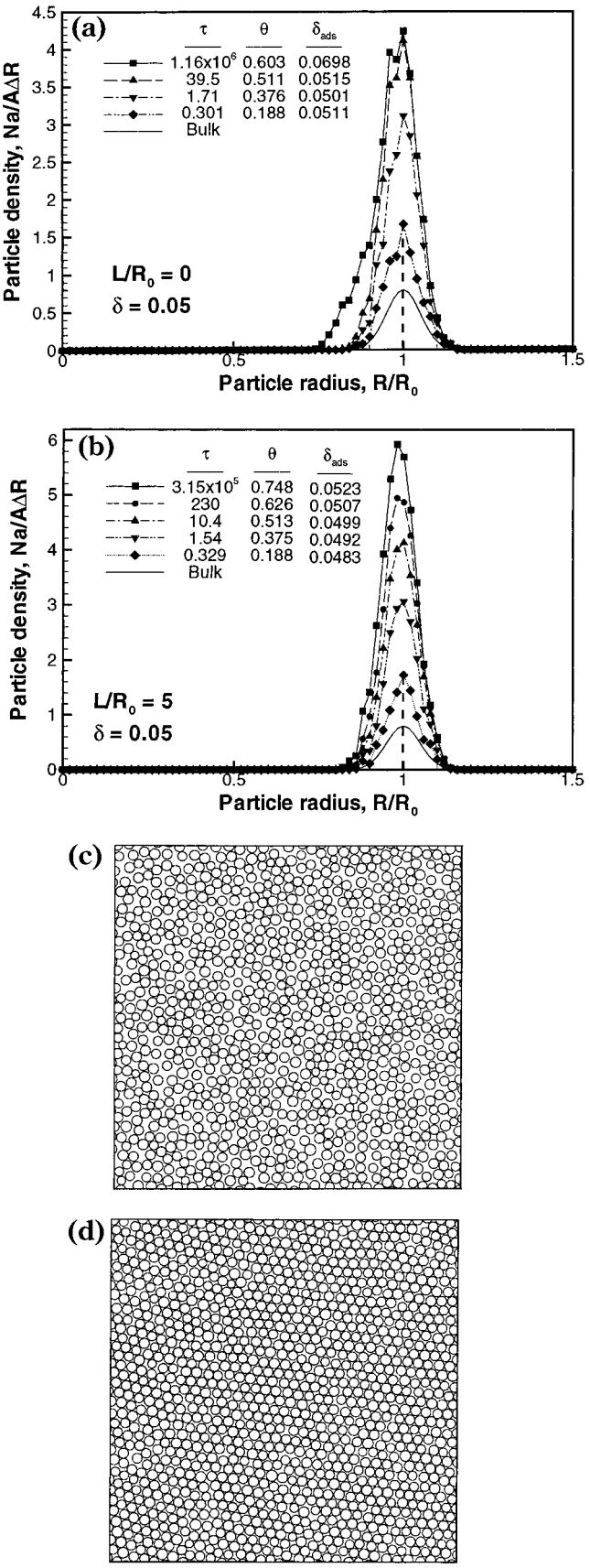

Figure 10. Time evolution of histograms and final surface structures for $\delta = 0.05$: (a,c) $L/R_0 = 0$ (liquid phase) and (b,d) $L/R_0 = 5$ (hexatic phase). Data are labeled by time τ, surface coverage θ, and surface polydispersity δ_{ads}. Bulk distributions shown for reference have been multiplied by 0.1 for viewing. Curves through data points are drawn using splines.

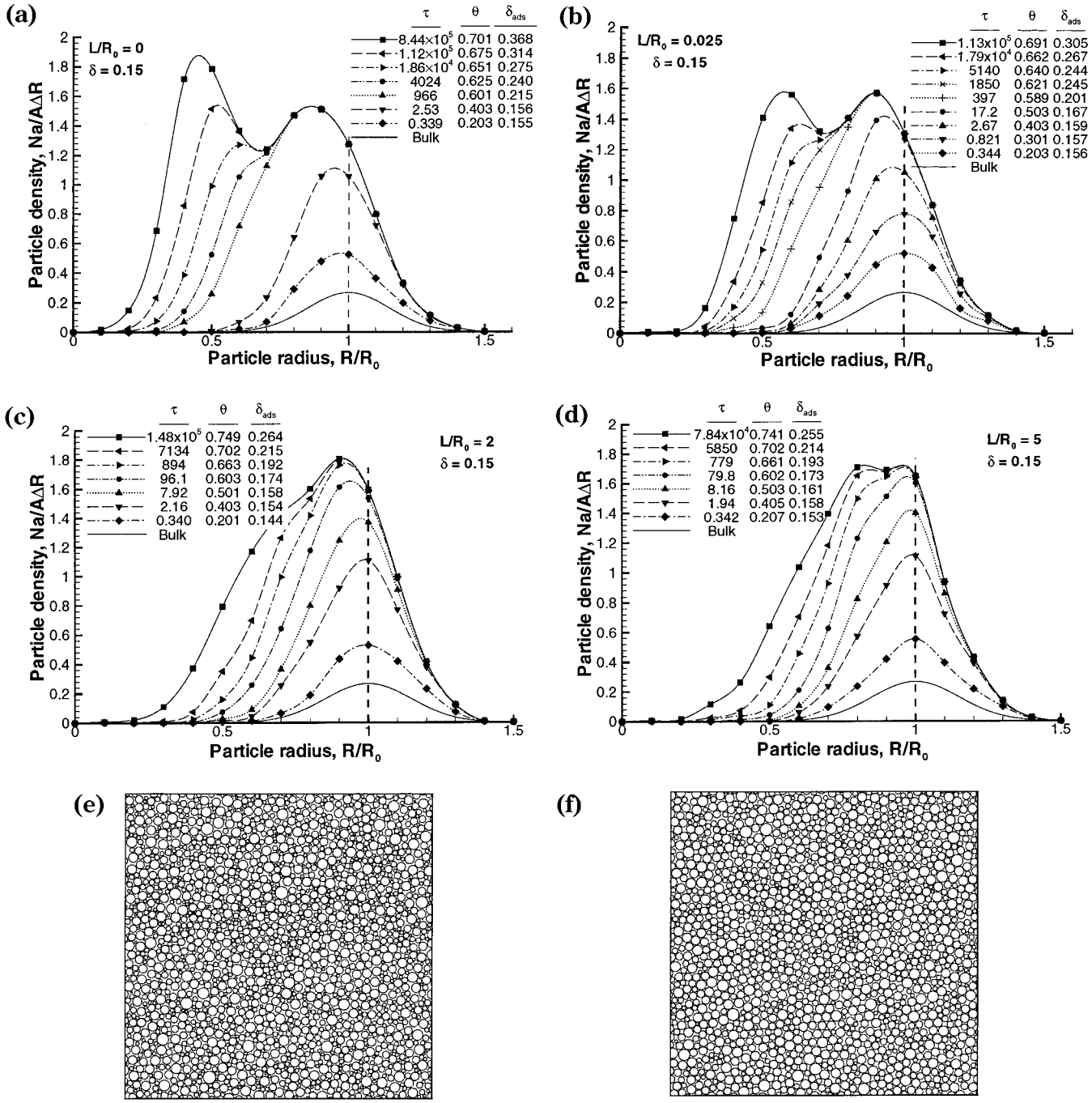

Figure 11. Time evolution of histograms of particle size distribution and final surface structures for $\delta = 0.15$: (a,e) $L/R_0 = 0$, (b) $L/R_0 = 0.25$, (c) $L/R_0 = 2$, and (d,f) $L/R_0 = 5$ (all surfaces are in the liquid phase). Data are labeled by time τ, surface coverage θ, and surface polydispersity δ_{ads}. Bulk distributions shown for reference have been multiplied by 0.1 for viewing. Curves through data points are drawn using splines.

sities. Figure 12 shows how the size distribution on the surface varies with δ at a fairly long time for $L/R_0 = 2$. At $\delta = 0.025$, the distribution remains Gaussian and thus symmetric. As polydispersity increases, the small end of the distribution widens. At 15% polydispersity, adsorbed particles range in size from 0.4 to $1.2R_0$. Figure 13 shows adsorbed particle polydispersity δ_{ads} plotted as a function of sample polydispersity in the bulk for several tether lengths. For polydispersities of 5% or less, the adsorbed phase has a similar polydispersity as the bulk phase. Larger polydispersities, however, affect the adsorbed distribution significantly. For polydispersities of 15% in the bulk, the adsorbed phase has a polydispersity ranging from 25% for long tethers to 31% for short tethers. "Short-tether behavior" (kinetic process) changes to "long-tether behavior" (near-equilibrium process) over $0 < L/R_0 < 1$, similar to phase behavior and kinetics.[4] For $L/R_0 > 1$, the tether length does not affect the relationship between the adsorbed phase polydispersity and the bulk polydispersity.

In general, surface polydispersity increases through time because of the preferential adsorption of small particles at long times. These increases can be dramatic, as Figure 14 shows. When $\delta \geq 0.07$, surface polydispersity, plotted as a function of surface coverage or time, is increasing dramatically at the time that the numerical simulations are stopped. However, only systems with large polydispersities increase in surface polydispersity. At this tether length ($L/R_0 = 2$), when $\delta \leq 0.05$, $\delta_{ads} \approx \delta$ for all times simulated; although there may be small gaps on

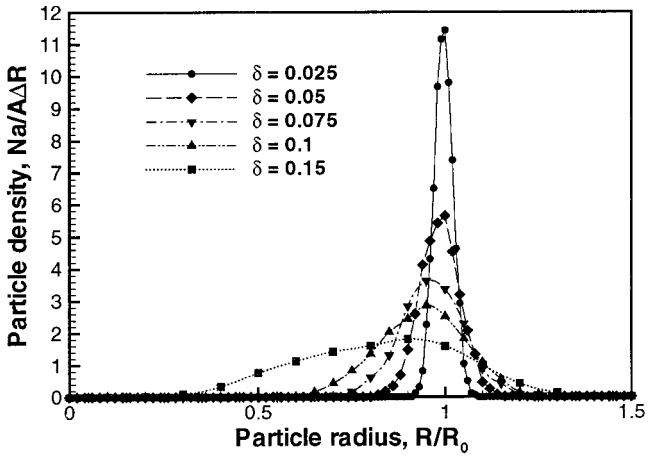

Figure 12. Histograms of particle size distribution as polydispersity is increased. $L/R_0 = 2$ and $\tau = 10^5$. Curves through data points are drawn using splines.

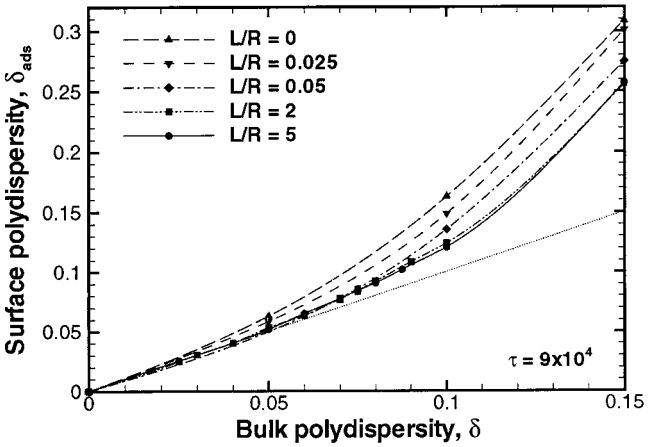

Figure 13. Adsorbed polydispersity versus bulk polydispersity for various tether lengths. For all data points, $\tau \approx 9 \times 10^4$. For reference, the dotted line represents $\delta = \delta_{ads}$.

the surface, the small polydispersity means that most of the particles are too large to fit into the gaps.

VI. Adsorption Kinetics and the Jamming Limit

The tether length and polydispersity impact the RSA kinetics. Figure 15 shows the fractional surface coverage versus time for monodisperse systems with three tether lengths and a 15% polydisperse system with no tethers. The polydisperse system behaves much like the $L/R_0 = 0.4$ system for times up to $\tau \approx 100$. After that, the coverage increases faster for the polydisperse system than for the monodisperse system. In fact, the slope of the kinetic curve for polydisperse particles appears strikingly similar to the case for monodisperse particles with infinite tethers. As the histograms of the last section showed, the small particles in a polydisperse system adsorb more frequently in the later stages of the process, which leads to the continually increasing coverage at long times.

Power-law behavior occurs at long times in classic RSA systems.[5,24] We fit long-time kinetic data to the asymptotic form

$$\theta = \theta_\infty - \alpha\tau^{-\beta} \tag{5}$$

to determine the kinetic constants α and β and the jamming limit θ_∞ by minimizing $(\theta_\infty - \theta - \alpha\tau^{-\beta})^2$ using the Nelder–Mead simplex (direct search) method. The kinetic data are plotted on logarithmic scales in Figure 16 along

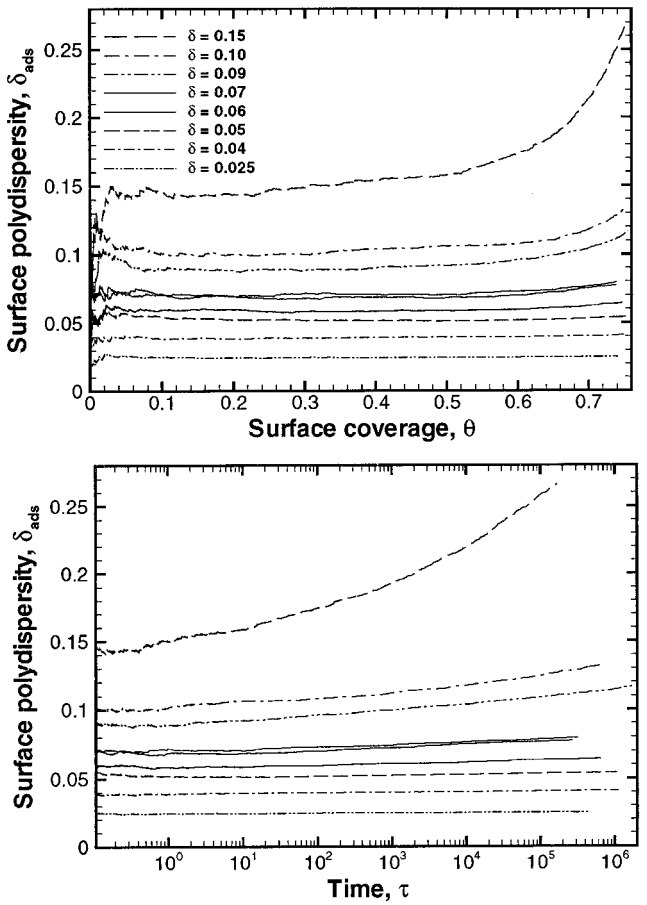

Figure 14. Surface phase polydispersity versus coverage (top) and time (bottom) for $L/R_0 = 2$ and various bulk polydispersities. Two independent runs are shown for $\delta = 0.07$.

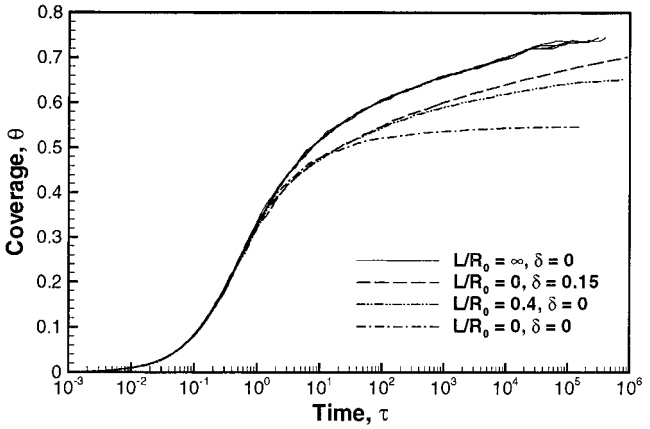

Figure 15. Coverage versus time for monodisperse and polydisperse systems. Three runs are shown for $L/R_0 = 4$ to show reproducibility.

with the power-law approximations for monodisperse and polydisperse systems with various tether lengths, revealing a fit over many orders of magnitude. The infinite tether case in Figure 16a shows that even when the kinetic data exhibits punctuated behavior as the surface reorganizes, the data follows the power law in an average sense.

One of the subtleties to fitting the power-law form is determining which data points to include in the fitting regime. Feder[5] fit the power law to all points after $\tau = 20$, and Swendsen[24] noted that the scalings should be valid at coverages above 0.4. Both of these measures approximate the point where the available space has been subdivided into individual triangles, the condition for

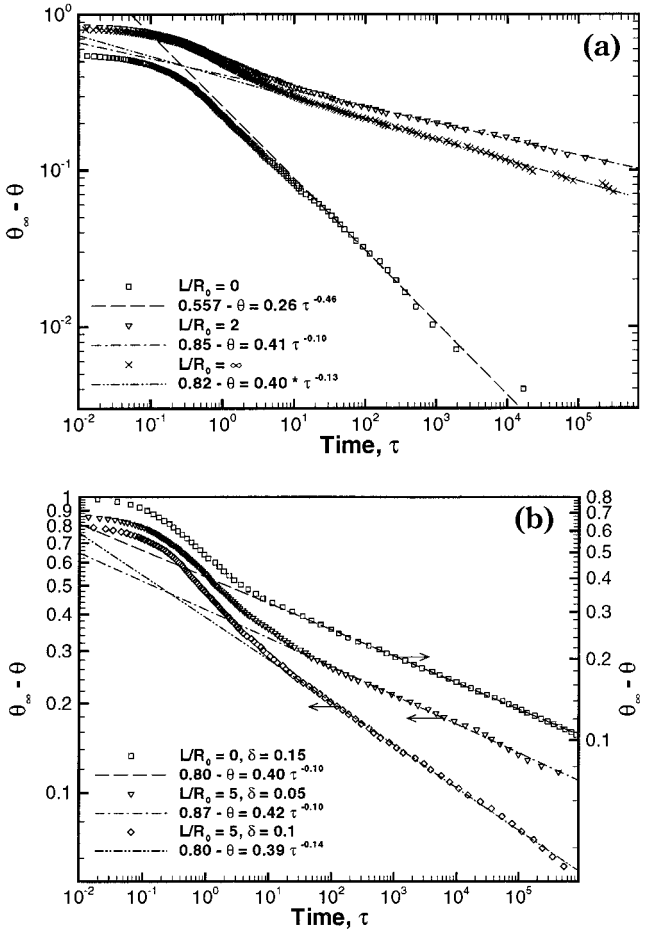

Figure 16. Power-law fits to data with $\tau \geq 30$ for (a) monodisperse and (b) polydisperse systems.

which the power-law form is derived.[24] In fact, we find that our constants vary somewhat as we change the initial time used in the fit, and, as might be expected, our fits are much better for runs with more long-time data. To quantify the error associated with the choice of the time interval, we fit the data using several different values for the initial time. The mean parameters over the set of fits are reported with the standard deviation as a measure of error. The error measure reflects both the amount of data collected and the quality of the power-law fit.

Figure 17 presents the power-law fits for various polydispersities and tether lengths, including the jamming limit extrapolations (Figure 17a). At $L/R_0 = 0$, jamming limit coverage increases nearly linearly with polydispersity from the classic RSA jamming limit of 0.547 to a nearly fully packed surface at $\delta = 0.2$ (similar to but more drastic than the linear increase for uniform distributions of particles[29]). At an intermediate tether length of $L/R_0 = 2$ (data shown in Figure 7), θ_∞ decreases from 0.85 to 0.8 as polydispersity is increased from 0 to 0.075 and increases again for larger polydispersities. At $L/R_0 = 5$, θ_∞ increases slightly from 0.82 to 0.84 for polydispersities from 0 to 0.06 and then drops sharply to near $\theta_\infty = 0.8$ before continuing a gentle increase at higher polydispersities.

Polydispersity creates two competing trends that affect the jamming coverage. First, the polydispersity allows the gaps on the surface to be filled by small particles, resulting in larger coverages for higher polydispersities in the zero-tether and longer tether cases. Second, the destruction of organization reduces the jamming coverage, in a relatively continuous way with the loss of hexatic

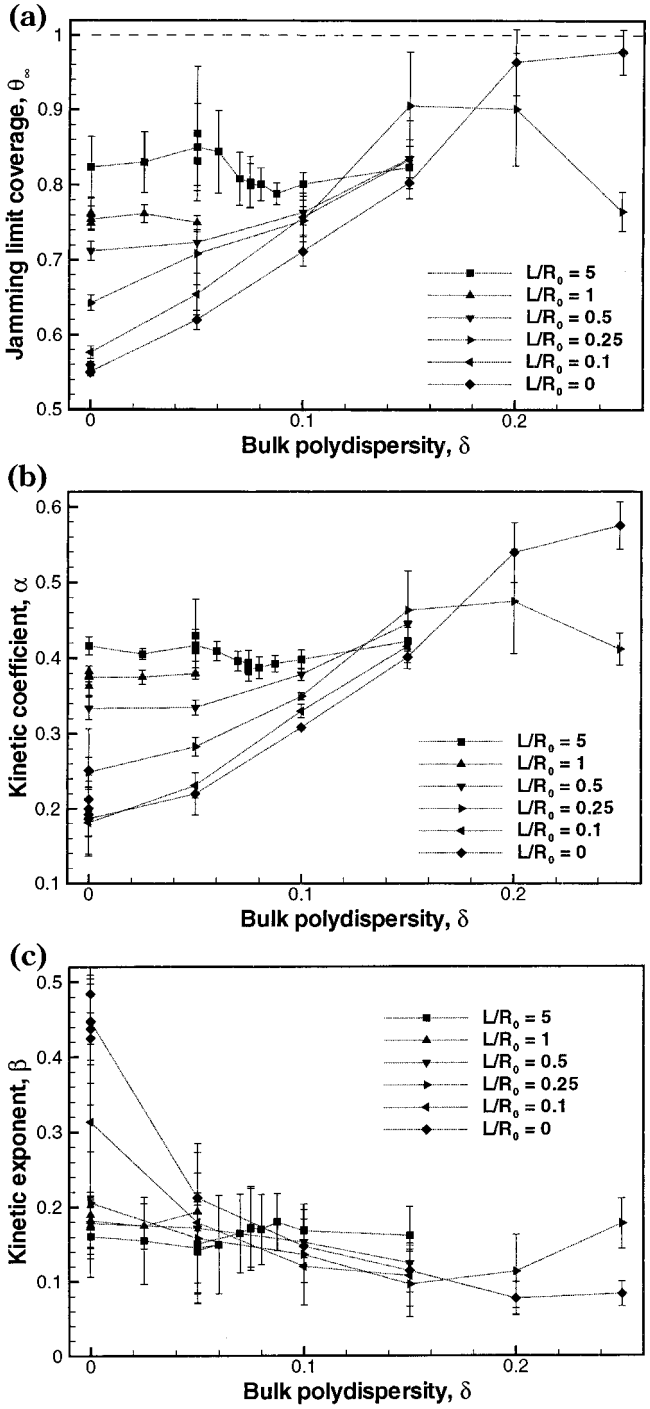

Figure 17. Effect of polydispersity and tether length on the kinetic parameters θ_∞, α, and β for the power-law fit of eq 5. Points and error bars represent the mean and standard deviation of a set of curve fits with different initial times. The set of initial times is $\tau_1 = \{1, 3, 10, 30, 100\}$ for all points except ($L/R_0 = 5$, $\delta = 0$) and ($L/R_0 = 0.025$, $\delta = 0.25$), where the set of initial times is $\tau_1 = \{1, 3, 10, 30\}$.

order in the $L/R = 2$ systems and in a more stepwise manner for the breakup of the crystalline $L/R_0 = 5$ cases.

As discussed in ref 4, these are jamming limits for a nonequilibrium system. Note that the jamming limits for the ordered $L/R_0 = 5$ cases are less than the close-packed monodisperse coverage of 0.9069, and all polydisperse cases are less than the limit coverage of unity for Apollonian packing. The ultimate configurations depend on the sequence of particle placement and the anchor locations. Also, thermal motions break up the perfect long-

range order necessary for maximal packing, in accordance with two-dimensional symmetry requirements.[43]

The kinetic coefficient α behaves similarly to θ_∞ (Figure 17b). For tether lengths of 0, α increases nearly linearly with polydispersity. α increases with tether length, and, like θ_∞, most variation with tether length occurs for $L/R_0 < 1$. The $L/R_0 = 5$ case shows a slight drop near the order−disorder phase boundary of $\delta \approx 0.075$.

Figure 17c presents the fits for the kinetic exponent β. Although our simulations of the classic RSA case exhibit $\beta = 0.45$ (comparable to the theoretical exponent of 0.5[24]), most of the other cases, both large polydispersities and long tethers, exhibit much slower behavior with $0.1 \leq \beta \leq 0.2$. Both surface mobility and polydispersity increase the system's degrees of freedom and reduce β in quantitatively similar ways. The similarity of the curves for infinite tether length and 15% polydispersity in Figure 15 attests to this. In general, β is smaller for larger polydispersities and longer tether lengths. One notable exception is the $L/R_0 = 5$ case which shows a distinct increase from 0.15 to 0.18 near the order−disorder transition at $\delta = 0.075$, indicating a faster approach to the jamming limit for the disordered surface. Also, the $L/R_0 = 0.1$ case shows an increase in β for very large polydispersities ($\delta > 0.15$).

Although predictions exist for β in polydisperse RSA,[25,27] there is no theoretical form for adsorption from a Gaussian distribution of particles. Our results compare well with previous simulation work. Meakin and Julien[28] found $\beta = 0.5$ to fit well for a very small polydispersity ($\delta = 0.0035$), and for a large polydispersity ($\delta = 0.124$), they found the exponent to be much smaller. However, they declined to specify a best-fit exponent for the case of large polydispersity, and others[29,35] similarly do not report exponents or long-time extrapolations.

Perhaps exponents have not been previously reported because they are difficult to obtain precisely, especially relative to the classic RSA case ($L/R_0 = 0$). Several factors may contribute to the accuracy of the estimates of the exponents. First, because of the slow kinetics of polydisperse tethered systems, computational capacity limits the number of runs performed. Whereas other studies routinely average results from up to 30 simulations, results here are reported for 1−5 repetitions. These repetitions are plotted individually for several cases (Figure 16c), and the scatter gives a measure of the precision of our fits. Second, lower values of β are favored because lower exponents tend to "flatten" the kinetic data, thus lowering the residual. This effect is underscored by the fact that in all five runs that we performed for the classic RSA case, the mean β is underpredicted (though the "correct" theoretical result of 0.5 is within the error limits). Third, for long tethers and large polydispersities, error is introduced by the large extrapolation distance to the jamming limit. For many cases, final simulation coverages are around 10% lower than the extrapolated jamming limit, whereas in the classic case it is easy to achieve coverages within 1% of the jamming limit. Nevertheless, the simulations are sufficient for determining long-time behavior within the error bars reported.

VII. Conclusions

We have simulated the random sequential adsorption of polydisperse tethered nanoparticles. Long tethers and fairly monodisperse particles are necessary for the formation of long-range ordered structures. Polydispersities of 5−8% break up crystalline or hexatic order. The adsorbed particle size distribution can significantly differ from the bulk size distribution as the adsorption of small particles is favored on disorganized layers, particularly for samples with a broad size distribution in the bulk. Bimodal size distributions occur for wide polydispersities, unless long tethers allow surface restructuring to close small gaps in the structure. Finally, we have extracted jamming limits and kinetic parameters including exponents for which no theoretical derivation is known.

Tethers allow the simulation to range from a completely kinetic process to a near-equilibrium one. For both polydisperse and monodisperse systems, many of the phenomena studied vary greatly as tether length is increased from 0 to R_0. When particles are given a small amount of freedom, liquid systems become hexatic, distributions of particles change, jamming limits increase, and kinetics become significantly slower. Apparently, many of these properties are very sensitive to local, short-range structure. In many cases, this is somewhat intuitive. For example, continued adsorption of new particles depends on the triangular gaps between preadsorbed particles. The local, three-body interactions on the surface strongly influence the size of these gaps and thus affect adsorption kinetics and the evolution of the particle size distribution on the surface.

Longer tether lengths give rise to long-range interactions and collective behavior that allows hexatic phases to evolve to crystal phases (for sufficiently low polydispersities). The necessity of crystal phases rather than hexatic phases in a nanoscale system will depend on the particular application. Indeed, in experimental work on nanoparticle superlattices, the distinction between hexatic and crystal systems is usually not noted, even when the characteristic twist of the hexatic can be seen in published photographs of monolayers of particles.

Experimental realization of the adsorption of tethered nanocrystals would be useful to validate our results and extend them to larger length and longer time scales. As noted in ref 4, simulations correspond roughly to hours of real time, depending on the system chosen. Our simulations use a large ratio of surface diffusion to adsorption (low Damkohler number) to be valid in the dilute suspension limit; however, in experiment the bulk particle volume fraction can be used to tune this ratio. There will be many challenges to create an experimental system to compare simulation results. Certainly, in the real three-dimensional world a tether would allow motion in the direction normal to the substrate as well as in the lateral direction. This may lead to particle stacking or the formation of multilayer structures, which, although not studied here, may also make interesting morphologies. It may be possible to minimize three-dimensional effects in experimental systems by designing for a delicate balance of interactions with the surface; van der Waals or electrostatic interactions between nanocrystals could keep particles on the surface, but steric layers could be used to maintain sufficient distance to prevent permanent deposition and allow lateral diffusion.

Appendix: Computation of Correlation Functions

Here, we describe the correlation functions used to quantify structure in the adsorbed surface layers. In the simulations, statistics are gathered after each of the $M = 100$ sets of diffusion procedures of 200 Monte Carlo cycles each. The correlation functions are evaluated by summing over particles in annular slices of width Δr (usually $\Delta r =$

(43) Chaikin, P. M.; Lubensky, T. C. *Principles of Condensed Matter Physics*; Cambridge University Press: New York, 1995.

$0.05R_0$) centered at radius r. Letting $r_1 = r - \Delta r/2$ and $r_2 = r + \Delta r/2$ be the boundaries of the annulus, the pair correlation function is

$$g(r) = \frac{2A \sum_{k=1}^{M} \sum_{i=1}^{N} \sum_{j=i+1}^{N} \delta(r_1 < r_{ij} < r_2)}{\pi(r_2^2 - r_1^2)\, MN^2} \qquad \text{(A-1)}$$

where A is the area of the simulation box, the first sum is over the M diffusion cycles, the second and third sums span all pairs of the N particles, r_{ij} is the distance between particles i and j, and the function δ counts 1 for the particle pairs that are within the specified annular region and 0 for all others.

Similarly, the orientational correlation function is

$$g_6(r) = \frac{2A \sum_{k=1}^{M} \sum_{i=1}^{N} \sum_{j=i+1}^{N} \mathrm{Re}\ \psi_6^{*(i)}\, \psi_6^{(j)}\, \delta(r_1 < r_{ij} < r_2)}{\pi(r_2^2 - r_1^2)\, MN^2} \qquad \text{(A-2)}$$

where $\psi_6^{(i)}$ and $\psi_6^{(j)}$ represent the orientational order parameters for particles i and j, respectively, as defined in eq 3, the star represents the complex conjugate, and Re represents taking the real part of the complex number.

LA001029J